THE JOURNAL OF PHYSICAL CHEMISTRY Letters

Letter

Cite This: J. Phys. Chem. Lett. 2018, 9, 2202−2207

pubs.acs.org/JPCL

Pressure-Induced Topological Phase Transitions in $CdGeSb_2$ and $CdSnSb_2$

Rinkle Juneja,[‡] Ravindra Shinde,[‡] and Abhishek K. Singh*

Materials Research Centre, Indian Institute of Science, Bangalore, Karnataka 560012, India

Supporting Information

ABSTRACT: Using first-principles calculations, we study the occurrence of topological quantum phase transitions (TQPTs) as a function of hydrostatic pressure in $CdGeSb_2$ and $CdSnSb_2$ chalcopyrites. At ambient pressure, both materials are topological insulators, having a finite band gap with inverted order of Sb-s and Sb-p_xp_y orbitals of valence bands at the Γ point. Under hydrostatic pressure, the band gap reduces, and at the critical point of the phase transition, these materials turn into Dirac semimetals. Upon further increasing the pressure beyond the critical point, the band inversion is reverted, making them trivial insulators. This transition is also captured by the Lüttinger model Hamiltonian, which demonstrates the critical role played by pressure-induced anisotropy in frontier bands in driving the phase transitions. These theoretical findings of peculiar coexistence of multiple topological phases provide a realistic and promising platform for experimental realization of the TQPTs.

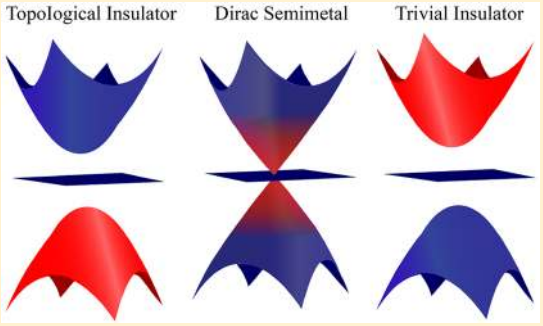

Topological insulators (TIs) have triggered a surge of research activities due to their peculiar properties. This intriguing state of matter is characterized by nonzero topological invariants and exhibits unique features such as an insulating gap in the bulk and robust metallic surface or edge Dirac states protected by time-reversal symmetry.[1−3] Until now, numerous two- and three-dimensional TIs were discovered with spin−orbit coupling (SOC)-induced parity inversion of conduction and valence bands as a guiding principle.[4−9]

Dirac semimetals (DSMs), on the other hand, have metallic states touching only at a single point near the Fermi energy with a linear band dispersion.[10−14] The bulk band gap of TIs too can be closed, thereby placing the topologically protected metallic bulk states at the critical point of a topological quantum phase transition (TQPT). This has been realized by tuning an intrinsic material's property such as spin−orbit interaction by alloying composition or chemical doping.[15−18] For example, a quantum critical transition from a TI to a trivial insulator has been observed in $TlBiSe_{2-x}S_x$[19,20] and $Hg_{1-x}Cd_xTe$,[21] where a single Dirac point occurs at the time-reversal-invariant momenta. The transition in these compounds is very sharp in terms of exact alloying concentration, and realizing an accurate, stable, homogeneous 3D Dirac material in these systems is an experimental challenge.[15,17,21]

These transitions can also be achieved through pressure without the need for any doping or alloying. Besides, this method circumvents the problem of unwanted defects and inhomogeneity of doping. Hence, it has become a popular tool for observing quantum phase transitions in topological materials. For example, strain-induced topological phase transition was studied for elemental tellurium[22] and HgSe.[23] Pressure-induced topological phase transition in rocksalt chalcogenides,[24] layered materials,[25] BiTeI,[26] $Pb_{1-x}Sn_xSe$,[27] and polar semiconductors BiTeBr[28] and BiTeI[29] was observed, while the TI phase in NaBaBi[30] and Zintl compounds[31] was obtained starting from a semimetallic state. The phase transition due to pressure was also observed in topological crystalline insulators.[32]

To observe the topological phase transition by detecting the gapless metallic surface states, surface-sensitive experimental techniques such as angle-resolved photoemission spectroscopy (ARPES) and scanning tunneling microscopy are used. However, performing ARPES to observe surface states at high pressures is a challenging task, making it experimentally difficult to study pressure-induced phase transitions in topological materials. On the other hand, the theoretical investigations provide a feasible alternative to probe these transitions, as well as to characterize the peculiar surface states simultaneously before performing any experiments. Hence, interest in the theoretical exploration of pressure-induced TQPTs has been renewed.

In this Letter, we report pressure-induced topological phase transitions in chalcopyrite compounds $CdGeSb_2$ and $CdSnSb_2$ by first-principles density functional based approach. These materials are small-band-gap TIs in their equilibrium states. The bulk band gap of these materials decreases upon application of pressure, and materials transform to a DSM at a critical pressure. The band gap reopens with a normal band

Received: March 1, 2018
Accepted: April 12, 2018
Published: April 12, 2018

DOI: 10.1021/acs.jpclett.8b00646
J. Phys. Chem. Lett. 2018, 9, 2202−2207

order above the critical pressure. We also simulate the ARPES at ambient pressure as well as at the critical point of TQPT using ab initio tight-binding calculations. These TQPTs are further substantiated by generalized model Hamiltonian calculations, which emulate the evolution of the band structure with the application of pressure. This model shows breaking of the spherical isotropic nature of bands and the emerging dominance of anisotropic terms as a function of pressure, thereby supporting the nontrivial-to-trivial phase transition. These theoretical investigations provide an ideal platform to study multitopological phase transitions in the same material and may serve as a guide for experimental realization.

Theoretical calculations were performed within the first-principles density functional theory (DFT)[33] using the Vienna ab initio simulation package (VASP).[34] Core electrons were represented by projector-augmented wave potentials.[35] Because PBE functional underestimates the band gap, it may not be applicable in the case of small-band-gap materials with strong SOC, particularly where materials are classified as TIs with a false band inversion. Hence, we used a hybrid HSE functional that takes 25% of the short-range exact exchange.[36]

Relativistic effects were included in the calculations with a plane-wave basis energy cutoff of 400 eV and a Γ-centered Monkhorst–Pack[37] **k**-grid of 5 × 5 × 5. All of the structures, after the application of hydrostatic pressure, were relaxed by employing a conjugate-gradient scheme until the forces on each atom became less than 0.005 eV/Å. The band structures were then calculated with and without SOC using these optimized structures.

The topological invariance, characterized by the $\mathbb{Z}_2$ number, was calculated by the method of evolution of Wannier charge centers (WCCs), as implemented in Z2Pack.[38] The charge centers of a given set of Wannier functions are defined as the average position of charge of a Wannier function in the chosen unit cell. The evolution of a WCC along any direction in *k*-space corresponds to the change in the phase factor θ of the eigenvalues of the position operator projected onto the occupied subspace.[38−40] The odd number of crossings of any random horizontal reference line with the evolution of θs signifies a TI with $\mathbb{Z}_2 = 1$. A tight-binding model was built based on maximally localized Wannier functions (MLWFs) obtained using ab initio DFT results. An iterative Green's function method was employed to obtain the surface density of states.[41,42] A generalized Lüttinger $j = 3/2$ model Hamiltonian was constructed to mimic the evolution of HSE bands with pressure.

Crystallographic Structure and Electronic Properties: The compounds studied here belong to the class of II–IV–V_2 materials that crystallize in the tetragonal chalcopyrite structure with $I\bar{4}2d$ space group.[43,44] In this structure, each of the group II and group IV elements is tetrahedrally coordinated by four group V elements while the group V elements are tetrahedrally coordinated by two group II and two group IV elements, as shown in Figure 1. Because the group V atom is bonded to two different types of cations, the respective bond lengths are not necessarily the same. Hence, the c/a ratio deviates from an ideal value of 2. The optimized lattice parameters for the $CdSnSb_2$ and $CdGeSb_2$ unit cells are $a = b = 6.63$ Å, $c = 13.11$ Å and $a = b = 6.45$ Å, $c = 12.48$ Å, respectively. The corresponding Brillouin zone with the high-symmetry points is also shown in Figure 1.

Figure 2 shows the HSE band structures of $CdSnSb_2$ and $CdGeSb_2$ without and with SOC. The inset shows the orbital

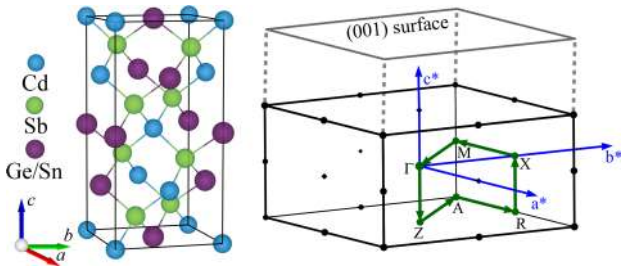

Figure 1. Conventional unit cell of II–IV–V_2 chalcopyrite compounds $CdGeSb_2$/$CdSnSb_2$ with a corresponding Brillouin zone and its projection onto the (001) surface along with high-symmetry points.

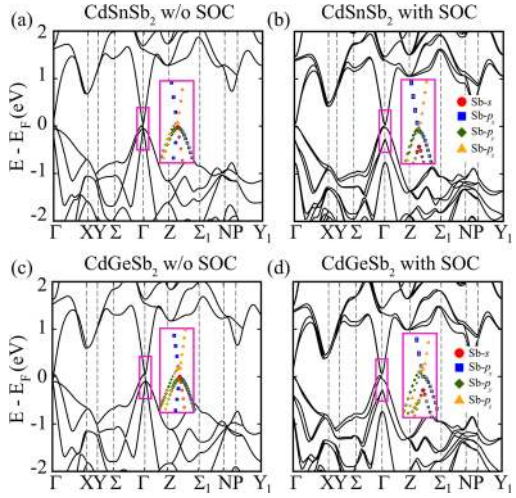

Figure 2. Orbital-resolved electronic band structures of $CdSnSb_2$ and $CdGeSb_2$ without and with SOC.

contribution of Sb atoms, which has a major contribution of orbitals in the vicinity of the Γ point for both compounds. In the absence of SOC, the valence band maximum (VBM) has the major contribution from Sb-s orbitals, followed by the bands with Sb-p_x and Sb-p_y contribution, whereas the conduction band minimum (CBM) has Sb-p_z character dominating, along with minor Sb-p_x and Sb-p_y contribution. Upon the inclusion of SOC, a small gap of 0.021 and 0.058 eV is opened for $CdSnSb_2$ and $CdGeSb_2$, respectively. Furthermore, the order of the valence bands gets inverted at the Γ point due to an interchange of Sb-s and Sb-p_x, Sb-p_y character, for both compounds. Hence, $CdSnSb_2$ and $CdGeSb_2$ are nontrivial TIs.

Because the nontrivial topological character should be reflected on the surface, we did Z-terminated (001) plane surface state calculations for $CdSnSb_2$ and $CdGeSb_2$, based on the idea of the bulk-edge correspondence of the TIs.[35] The surface density of states with SOC, calculated using an iterative Green's function method, is shown in panels (a,b) and (c,d) of Figure 3 for the ambient pressure phase and at the critical pressure, respectively. The tight-binding model based on the MLWFs correctly reproduces the DFT band structure and simulates the ARPES with the calculated surface density of states. The energy dispersion in two dimensions at the critical pressure for both materials is shown in Figure 4. To further confirm the topological nature of both compounds, we also calculated the $\mathbb{Z}_2$ topological invariant through the evolution of WCCs. The $\mathbb{Z}_2$ for these compounds comes out to be 1, thereby substantiating their nontrivial topology.

DOI: 10.1021/acs.jpclett.8b00646
J. Phys. Chem. Lett. 2018, 9, 2202−2207

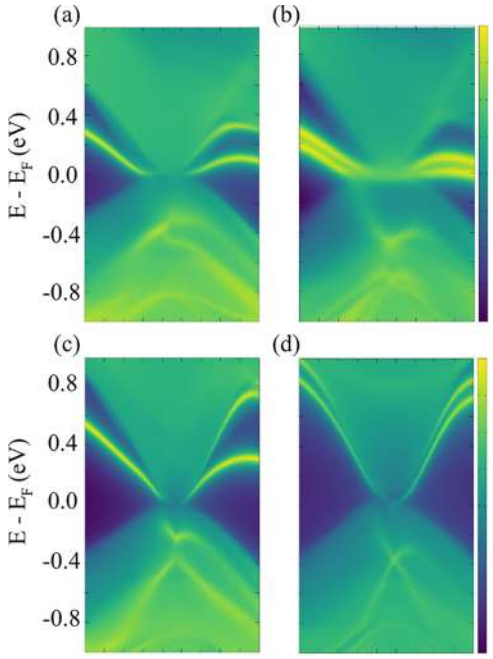

Figure 3. Momentum-resolved (001) surface density of states for $CdSnSb_2$ and $CdGeSb_2$ with SOC (a,b) in the equilibrium phase and (c,d) at the critical point under hydrostatic pressure, respectively. Surface states are seen connecting at the Dirac point.

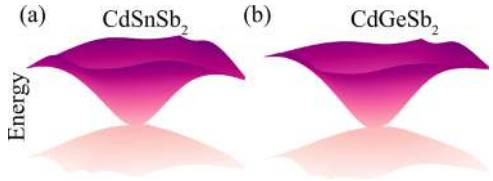

Figure 4. Two-dimensional energy dispersion of (a) $CdSnSb_2$ and (b) $CdGeSb_2$ at the critical point.

The authors of refs 45 and 46 have also predicted these materials to be TIs in their equilibrium state with slightly larger band gaps. This disparity might have arisen because the authors[45,46] took an ideal chalcopyrite structure with $c/a = 2.0$, thereby overestimating the strain.

Effect of Hydrostatic Pressure: Next, we analyzed how the electronic structures of $CdSnSb_2$ and $CdGeSb_2$ change under hydrostatic compression. We applied hydrostatic compression in the pressure range of 0−8 GPa. All of the structures are dynamically stable in their TI, DSM, and semiconducting phases (Supporting Information Figure S1). Furthermore, ref 47 reports the first structural phase transition at 15 GPa for $CdSnSb_2$, whereas all of the electronic phase transitions occur at pressures well below this structural phase transition pressure. Figure 5a,b shows the evolution of the bulk energy band structure under hydrostatic pressure for $CdSnSb_2$ and $CdGeSb_2$, respectively. With increasing pressure, the band structures for both materials undergo similar interesting changes. As discussed earlier, at ambient pressure, the valence bands have a major contribution from Sb-p_x and Sb-p_y orbitals followed by the bands with s contribution, and the conduction bands have major Sb-p_z contribution. As the pressure increases, the band gap starts to reduce while keeping the order of other bands intact and becomes completely zero at the critical pressure of 2.21 and 2.30 GPa for $CdSnSb_2$ and $CdGeSb_2$, respectively. Hence, at low pressures, both compounds remain TIs with an inverted band order. As compression increases, a TQPT occurs, and the compounds turn to a DSM state at the critical pressures. Figures 3c,d show the calculated surface density of states at the critical pressure. Nontrivial edge states merging at the Dirac point can be contrasted with the trivial bulk states. Interestingly, upon further increasing the pressure above this critical point, the energy gap starts to increase along with the change in the character of bands. After the critical pressure, the valence and conduction bands have a major contribution from Sb-p_z, and Sb-s orbitals, respectively, which is

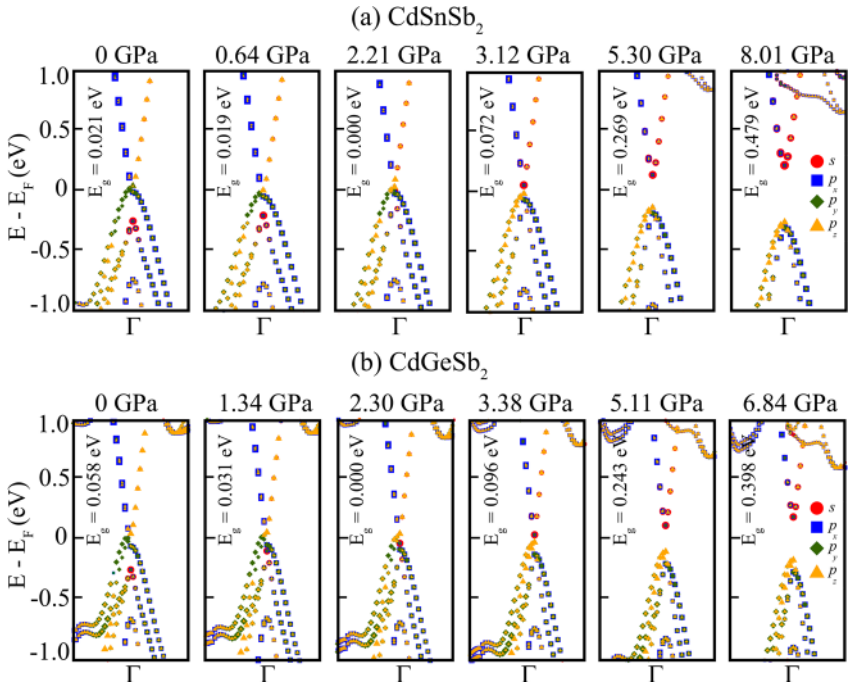

Figure 5. Effect of hydrostatic pressure on the band structures of (a) $CdSnSb_2$ and (b) $CdGeSb_2$.

DOI: 10.1021/acs.jpclett.8b00646
J. Phys. Chem. Lett. 2018, 9, 2202−2207

an inverted order compared to that of the ambient phase. The topological invariant $\mathbb{Z}_2$ above the critical point comes out to be zero, thereby confirming the TQPT.

Model Hamiltonian: Because the orbitals *s* and p have a major contribution around the Γ point at the Fermi level, a four-band modified Lüttinger model[48] Hamiltonian is constructed in the basis of $|\mathrm{Sb}_J, j_z\rangle = \left|\mathrm{Sb}_{3/2}, \pm\frac{3}{2}\right\rangle$ and $\left|\mathrm{Sb}_{3/2}, \pm\frac{1}{2}\right\rangle$. Mostly, these four states consist of the bonding and antibonding of s and p orbitals of Sb atoms. The Hamiltonian is given by

$$H = \frac{\hbar^2}{2m_0}(\alpha_1\mathbf{k}^2 I^0 + \alpha_2(\mathbf{k}\cdot\mathbf{J})^2 + \alpha_3 \sum \mathbf{k}^2\mathbf{J}^2 + \alpha_4) \quad (1)$$

where I^0 is a 4 × 4 identity matrix, and $\mathbf{J} = (J_x, J_y, J_z)$, with J_i being the 3/2 angular momentum matrices. The coefficients α_i are Lüttinger empirical parameters obtained by fitting them with the HSE band structure. At the Γ point, the degeneracy of all four bands is lifted by introducing a band gap-dependent term α_4. The first term with a quadratic order in momentum in eq 1 is invariant under spherical symmetry with inversion, representing the isotropic nature of the bands. The second and third terms introduce anisotropy in the bands, lowering the symmetry.

In the presence of SOC, the above Hamiltonian can be represented by

$$H = \begin{pmatrix} H_{11} & H_{12} & H_{13} & H_{14} \\ H_{12}^* & H_{22} & H_{23} & H_{24} \\ H_{13}^* & H_{23}^* & H_{33} & H_{34} \\ H_{14}^* & H_{24}^* & H_{34}^* & H_{44} \end{pmatrix}$$

where

$$H_{11} = \left(\alpha_1 - \frac{3}{4}\alpha_3\right)(k_x^2 + k_y^2) + \left(\alpha_1 - \frac{9}{4}\alpha_3\right)k_z^2 - 3\alpha_2 k_z + \alpha_4 \quad (2)$$

$$H_{12} = -\sqrt{3}\,\alpha_2(k_x - \mathrm{i}k_y) \quad (3)$$

$$H_{13} = -\frac{\sqrt{3}}{2}\alpha_3(k_x^2 - k_y^2) \quad (4)$$

$$H_{14} = 0 \quad (5)$$

$$H_{22} = \left(\alpha_1 - \frac{7}{4}\alpha_3\right)(k_x^2 + k_y^2) + \left(\alpha_1 - \frac{1}{4}\alpha_3\right)k_z^2 - \alpha_2 k_z + \alpha_4 \quad (6)$$

$$H_{23} = -2\alpha_2(k_x - \mathrm{i}k_y) \quad (7)$$

$$H_{24} = -\frac{\sqrt{3}}{2}\alpha_3(k_x^2 - k_y^2) \quad (8)$$

$$H_{33} = \left(\alpha_1 - \frac{7}{4}\alpha_3\right)(k_x^2 + k_y^2) + \left(\alpha_1 - \frac{1}{4}\alpha_3\right)k_z^2 + \alpha_2 k_z + \alpha_4 \quad (9)$$

$$H_{34} = -\sqrt{3}\,\alpha_2(k_x - \mathrm{i}k_y) \quad (10)$$

$$H_{44} = \left(\alpha_1 - \frac{3}{4}\alpha_3\right)(k_x^2 + k_y^2) + \left(\alpha_1 - \frac{9}{4}\alpha_3\right)k_z^2 + 3\alpha_2 k_z + \alpha_4 \quad (11)$$

Diagonalization gives two sets of degenerate bands that form valence and conduction bands. Figure 6 shows the fitted bands

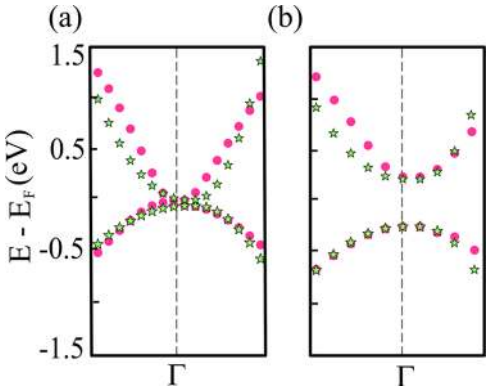

Figure 6. Lüttinger band structure for $CdSnSb_2$ fitted to HSE band structure for (a) ambient and (b) 8.01 GPa hydrostatic pressure.

at ambient pressure and 8.01 GPa. The corresponding parameters are listed in Table 1. While the isotropic term remains unchanged, the second and third terms in the eq 1 vary profoundly with pressure, signaling an enhancement of the anisotropy of bands.

Table 1. Lüttinger Parameters

pressure	α_1 (Å² eV)	α_2 (Å² eV)	α_3 (Å² eV)	α_4 (eV)
ambient	46	−19	−11	0.03
8.01 GPa	46	−40	11	0.23

The tunable Lüttinger parameters α_1, α_2, and α_3 in eq 1 scale the mass of the electron. For instance, the diagonal components of the effective mass tensors can be qualitatively related to α_1 via $m^* = m_0/\alpha_1$. Similar expressions for other diagonal and off-diagonal contributions to the effective mass tensor elements can be deduced from the values of α_2 and α_3. Due to the coupling of cross-terms of momenta, the anharmonicity dominates, leading to an increase in off-diagonal terms in the effective mass tensor. These tensors for the ambient phase, Dirac semimetallic phase, and normal semiconductor phase are given in the Supporting Information. The effective masses in certain directions increase, while in some directions they decrease, suggesting a buildup of anharmonicity.

The bands for the intermediate pressure values can be obtained by varying the parameters, which are listed in Table 1. Proper strain engineering enables control of the topological order. With a suitable choice of parameters, this model can be further extended to study the topological phase transition in a wide range of materials.

In summary, we have performed first-principles calculations to study the topological phase transitions in chalcopyrite compounds as a function of hydrostatic pressure. These compounds are TIs in the native phase with an inverted band order around the BZ center. Upon hydrostatic compression, there is a transition from a nontrivial TI phase to a Dirac semimetallic state at a critical pressure. Further increase in pressure drives the material into a trivial semiconductor along with normal ordering of bands. Different quantum phases are

DOI: 10.1021/acs.jpclett.8b00646
J. Phys. Chem. Lett. 2018, 9, 2202−2207

characterized by topological invariants as well as surface states. These quantum phase transitions are further validated by model calculations based on the Lüttinger Hamiltonian, which unravels the critical role played by the pressure-induced anisotropy of frontier bands in driving the phase transitions. Such a maneuver between various topological phases by hydrostatic pressure can stimulate the search for TQPTs in future experiments.

■ ASSOCIATED CONTENT

Supporting Information

The Supporting Information is available free of charge on the ACS Publications website at DOI: 10.1021/acs.jpclett.8b00646.

Phonon dispersion of compounds at various pressure values and effective mass tensors of $CdSnSb_2$ at three different phases (PDF)

■ AUTHOR INFORMATION

Corresponding Author

*E-mail: abhishek@iisc.ac.in.

ORCID

Ravindra Shinde: 0000-0001-5182-1480

Abhishek K. Singh: 0000-0002-7631-6744

Author Contributions

‡R.J. and R.S. contributed equally.

Notes

The authors declare no competing financial interest.

■ ACKNOWLEDGMENTS

R.S. acknowledges the Science and Engineering Research Board, India for a fellowship (PDF/2015/000466). R.J. thanks DST for an INSPIRE fellowship (IF150848). This work is partly supported by U.S. Army Contract FA5209-16-P-0090 and DST Nanomission. We also acknowledge MRC and SERC, IISc for providing the computational facilities.

■ REFERENCES

(1) Kane, C. L.; Mele, E. J. Z_2 Topological Order and the Quantum Spin Hall Effect. *Phys. Rev. Lett.* **2005**, *95*, 146802.

(2) Fu, L.; Kane, C. L.; Mele, E. J. Topological Insulators in Three Dimensions. *Phys. Rev. Lett.* **2007**, *98*, 106803.

(3) Hasan, M. Z.; Kane, C. L. Colloquium: Topological Insulators. *Rev. Mod. Phys.* **2010**, *82*, 3045.

(4) Bernevig, B. A.; Hughes, T. L.; Zhang, S.-C. Quantum Spin Hall Effect and Topological Phase Transition in HgTe Quantum Wells. *Science* **2006**, *314*, 1757−1761.

(5) Hsieh, D.; Qian, D.; Wray, L.; Xia, Y.; Hor, Y. S.; Cava, R. J.; Hasan, M. Z. A Topological Dirac Insulator in a Quantum Spin Hall Phase. *Nature* **2008**, *452*, 970−974.

(6) Teo, J. C. Y.; Fu, L.; Kane, C. L. Surface States and Topological Invariants in Three-Dimensional Topological Insulators: Application to $Bi_{1-x}Sb_x$. *Phys. Rev. B* **2008**, *78*, 045426.

(7) Zhang, H.; Liu, C.-X.; Qi, X.-L.; Dai, X.; Fang, Z.; Zhang, S.-C. Topological Insulators in Bi_2Se_3, Bi_2Te_3 and Sb_2Te_3 with a Single Dirac Cone on the Surface. *Nat. Phys.* **2009**, *5*, 438−442.

(8) Chen, Y. L.; Analytis, J. G.; Chu, J.-H.; Liu, Z. K.; Mo, S.-K.; Qi, X. L.; Zhang, H. J.; Lu, D. H.; Dai, X.; Fang, Z.; et al. Experimental Realization of a Three-Dimensional Topological Insulator, Bi_2Te_3. *Science* **2009**, *325*, 178−181.

(9) Qi, X.-L.; Zhang, S.-C. Topological Insulators and Superconductors. *Rev. Mod. Phys.* **2011**, *83*, 1057−1110.

(10) Liu, Z. K.; Zhou, B.; Zhang, Y.; Wang, Z. J.; Weng, H. M.; Prabhakaran, D.; Mo, S.-K.; Shen, Z. X.; Fang, Z.; Dai, X.; et al. Discovery of a Three-Dimensional Topological Dirac Semimetal, Na_3Bi. *Science* **2014**, *343*, 864−867.

(11) Neupane, M.; Xu, S.-Y.; Sankar, R.; Alidoust, N.; Bian, G.; Liu, C.; Belopolski, I.; Chang, T.-R.; Jeng, H.-T.; Lin, H. Observation of a Three-Dimensional Topological Dirac Semimetal Phase in High-Mobility Cd_3As_2. *Nat. Commun.* **2014**, *5*, 3786.

(12) Wang, Z.; Sun, Y.; Chen, X.-Q.; Franchini, C.; Xu, G.; Weng, H.; Dai, X.; Fang, Z. Dirac Semimetal and Topological Phase Transitions in A_3Bi (A = Na, K, Rb). *Phys. Rev. B* **2012**, *85*, 195320.

(13) Yang, B.-J.; Nagaosa, N. Classification of Stable Three-Dimensional Dirac Semimetals with Nontrivial Topology. *Nat. Commun.* **2014**, *5*, 4898.

(14) Gupta, S.; Juneja, R.; Shinde, R.; Singh, A. K. Topologically Nontrivial Electronic States in $CaSn_3$. *J. Appl. Phys.* **2017**, *121*, 214901.

(15) Brahlek, M.; Bansal, N.; Koirala, N.; Xu, S.-Y.; Neupane, M.; Liu, C.; Hasan, M. Z.; Oh, S. Topological-Metal to Band-Insulator Transition in $(Bi_{1-x}In_x)_2Se_3$ Thin Films. *Phys. Rev. Lett.* **2012**, *109*, 186403.

(16) Sato, T.; Segawa, K.; Kosaka, K.; Souma, S.; Nakayama, K.; Eto, K.; Minami, T.; Ando, Y.; Takahashi, T. Unexpected Mass Acquisition of Dirac Fermions at the Quantum Phase Transition of a Topological Insulator. *Nat. Phys.* **2011**, *7*, 840−844.

(17) Wu, L.; Brahlek, M.; Valdes Aguilar, R.; Stier, A. V.; Morris, C. M.; Lubashevsky, Y.; Bilbro, L. S.; Bansal, N.; Oh, S.; Armitage, N. P. A Sudden Collapse in the Transport Lifetime Across the Topological Phase Transition in $(Bi_{1-x}In_x)_2Se_3$. *Nat. Phys.* **2013**, *9*, 410−414.

(18) Yan, C.; Liu, J.; Zang, Y.; Wang, J.; Wang, Z.; Wang, P.; Zhang, Z.-D.; Wang, L.; Ma, X.; Ji, S. Experimental Observation of Dirac-like Surface States and Topological Phase Transition in $Pb_{1-x}Sn_xTe(111)$ Films. *Phys. Rev. Lett.* **2014**, *112*, 186801.

(19) Novak, M.; Sasaki, S.; Segawa, K.; Ando, Y. Large Linear Magnetoresistance in the Dirac Semimetal TlBiSSe. *Phys. Rev. B* **2015**, *91*, 041203.

(20) Singh, B.; Sharma, A.; Lin, H.; Hasan, M. Z.; Prasad, R.; Bansil, A. Topological Electronic Structure and Weyl Semimetal in the $TlBiSe_2$ Class of Semiconductors. *Phys. Rev. B* **2012**, *86*, 115208.

(21) Orlita, M.; Basko, D. M.; Zholudev, M. S.; Teppe, F.; Knap, W.; Gavrilenko, V. I.; Mikhailov, N. N.; Dvoretskii, S. A.; Neugebauer, P.; Faugeras, C.; et al. Observation of Three-Dimensional Massless Kane Fermions in a Zinc-Blende Crystal. *Nat. Phys.* **2014**, *10*, 233−238.

(22) Agapito, L. A.; Kioussis, N.; Goddard, W. A.; Ong, N. P. Novel Family of Chiral-Based Topological Insulators: Elemental Tellurium under Strain. *Phys. Rev. Lett.* **2013**, *110*, 176401.

(23) Winterfeld, L.; Agapito, L. A.; Li, J.; Kioussis, N.; Blaha, P.; Chen, Y. P. Strain-Induced Topological Insulator Phase Transition in HgSe. *Phys. Rev. B* **2013**, *87*, 075143.

(24) Barone, P.; Rauch, T.; Di Sante, D.; Henk, J.; Mertig, I.; Picozzi, S. Pressure-Induced Topological Phase Transitions in Rocksalt Chalcogenides. *Phys. Rev. B* **2013**, *88*, 045207.

(25) Zhu, Z.; Cheng, Y.; Schwingenschlögl, U. Topological Phase Transition in Layered GaS and GaSe. *Phys. Rev. Lett.* **2012**, *108*, 266805.

(26) Xi, X.; Ma, C.; Liu, Z.; Chen, Z.; Ku, W.; Berger, H.; Martin, C.; Tanner, D. B.; Carr, G. L. Signatures of a Pressure-Induced Topological Quantum Phase Transition in BiTeI. *Phys. Rev. Lett.* **2013**, *111*, 155701.

(27) Xi, X.; He, X.-G.; Guan, F.; Liu, Z.; Zhong, R. D.; Schneeloch, J. A.; Liu, T. S.; Gu, G. D.; Du, X.; Chen, Z. Bulk Signatures of Pressure-Induced Band Inversion and Topological Phase Transitions in $Pb_{1-x}Sn_xSe$. *Phys. Rev. Lett.* **2014**, *113*, 096401.

(28) Ohmura, A.; Higuchi, Y.; Ochiai, T.; Kanou, M.; Ishikawa, F.; Nakano, S.; Nakayama, A.; Yamada, Y.; Sasagawa, T. Pressure-Induced Topological Phase Transition in the Polar Semiconductor BiTeBr. *Phys. Rev. B* **2017**, *95*, 125203.

(29) Park, J.; Jin, K.-H.; Jo, Y. J.; Choi, E. S.; Kang, W.; Kampert, E.; Rhyee, J.-S.; Jhi, S.-H.; Kim, J. S. Quantum Oscillation Signatures of Pressure-induced Topological Phase Transition in BiTeI. *Sci. Rep.* **2015**, *5*, 15973.

DOI: 10.1021/acs.jpclett.8b00646
J. Phys. Chem. Lett. 2018, 9, 2202−2207

(30) Sun, Y.; Wang, Q.-Z.; Wu, S.-C.; Felser, C.; Liu, C.-X.; Yan, B. Pressure-Induced Topological Insulator in NaBaBi with Right-Handed Surface Spin Texture. *Phys. Rev. B* **2016**, *93*, 205303.
(31) Zhu, Z.; Li, M.; Li, J. Topological Semimetal to Insulator Quantum Phase Transition in the Zintl Compounds Ba_2X(X = Si, Ge). *Phys. Rev. B* **2016**, *94*, 155121.
(32) Zhao, L.; Wang, J.; Gu, B.-L.; Duan, W. Tuning Surface Dirac Valleys by Strain in Topological Crystalline Insulators. *Phys. Rev. B* **2015**, *91*, 195320.
(33) Kohn, W.; Sham, L. J. Self-Consistent Equations Including Exchange and Correlation Effects. *Phys. Rev.* **1965**, *140*, A1133.
(34) (a) Kresse, G.; Furthmüller, J. Efficiency of Ab-Initio Total Energy Calculations for Metals and Semiconductors Using a Plane-Wave Basis Set. *Comput. Mater. Sci.* **1996**, *6*, 15−50. (b) Kresse, G.; Furthmüller, J. Efficient Iterative Schemes for ab initio Total-Energy Calculations using a Plane-Wave Basis Set. *Phys. Rev. B* **1996**, *54*, 11169−11186.
(35) (a) Blöchl, P. E. Projector Augmented-Wave Method. *Phys. Rev. B* **1994**, *50*, 17953. (b) Kresse, G.; Joubert, D. From Ultrasoft Pseudopotentials to the Projector Augmented-Wave Method. *Phys. Rev. B* **1999**, *59*, 1758.
(36) (a) Heyd, J.; Scuseria, G. E.; Ernzerhof, M. Hybrid Functionals Based on a Screened Coulomb Potential. *J. Chem. Phys.* **2003**, *118*, 8207−8215. (b) Heyd, J.; Scuseria, G. E.; Ernzerhof, M. Erratum: "Hybrid Functionals Based on a Screened Coulomb Potential" [J. Chem. Phys. 118, 8207 (2003)]. *J. Chem. Phys.* **2006**, *124*, 219906.
(37) Monkhorst, H. J.; Pack, J. D. Special Points for Brillouin-Zone Integrations. *Phys. Rev. B* **1976**, *13*, 5188.
(38) Soluyanov, A. A.; Vanderbilt, D. Computing Topological Invariants without Inversion Symmetry. *Phys. Rev. B* **2011**, *83*, 235401.
(39) Fu, L.; Kane, C. L. Time Reversal Polarization and a Z_2 Adiabatic Spin Pump. *Phys. Rev. B* **2006**, *74*, 195312.
(40) Yu, R.; Qi, X. L.; Bernevig, A.; Fang, Z.; Dai, X. Equivalent Expression of Z_2 Topological Invariant for Band Insulators using the Non-Abelian Berry Connection. *Phys. Rev. B* **2011**, *84*, 075119.
(41) Mostofi, A. A.; Yates, J. R.; Pizzi, G.; Lee, Y.-S.; Souza, I.; Vanderbilt, D.; Marzari, N. An Updated Version of Wannier90: A Tool for Obtaining Maximally-Localised Wannier Functions. *Comput. Phys. Commun.* **2014**, *185*, 2309−2310.
(42) Wu, Q.; Zhang, S.; Song, H.-F.; Troyer, M.; Soluyanov, A. A. WannierTools: An Open-Source Software Package for Novel Topological Materials. *Comput. Phys. Commun.* **2018**, *224*, 405−416.
(43) Tengå, A.; García-García, F. J.; Mikhaylushkin, A. S.; Espinosa-Arronte, B.; Andersson, M.; Häussermann, U. Sphalerite-Chalcopyrite Polymorphism in Semimetallic $ZnSnSb_2$. *Chem. Mater.* **2005**, *17*, 6080−6085.
(44) Shay, J. L.; Wernick, J. H. *Ternary Chalcopyrite Semiconductors: Growth, Electronic Properties, and Applications: International Series of Monographs in The Science of The Solid State*; Elsevier, 2013; Vol. 7.
(45) Feng, W.; Xiao, D.; Ding, J.; Yao, Y. Three-Dimensional Topological Insulators in I-III-VI_2 and II-IV-V_2 Chalcopyrite Semiconductors. *Phys. Rev. Lett.* **2011**, *106*, 016402.
(46) Feng, W.; Yao, Y. Three-Dimensional Topological Insulators: A Review on Host Materials. *Sci. China: Phys., Mech. Astron.* **2012**, *55*, 2199−2212.
(47) Hu, J.; Shi, L.; Qin, Y.; Jin, F.; Duan, Y.; Qiu, L.; Chen, L. Phase Transitions, Band Structures, Elastic and Lattice Dynamic Properties of $CdSnV_2$ (V = P, As, Sb) under Pressure from First-Principles. *Mater. Sci. Semicond. Process.* **2015**, *35*, 149−161.
(48) Lüttinger, J. M. Quantum Theory of Cyclotron Resonance in Semiconductors: General Theory. *Phys. Rev.* **1956**, *102*, 1030−1041.

DOI: 10.1021/acs.jpclett.8b00646
J. Phys. Chem. Lett. 2018, 9, 2202−2207